Quantum Hypercube States

L. A. Howard,[1] T. J. Weinhold,[1] F. Shahandeh,[2] J. Combes,[1] M. R. Vanner,[3] A. G. White,[1] and M. Ringbauer[4]
[1]*Centre for Engineered Quantum Systems, School of Mathematics and Physics, University of Queensland, Brisbane, Australia*
[2]*Department of Physics, Swansea University, Singleton Park, Swansea SA2 8PP, United Kingdom*
[3]*QOLS, Blackett Laboratory, Imperial College London, London, United Kingdom*
[4]*Institut für Experimentalphysik, Universität Innsbruck, 6020 Innsbruck, Austria*

(Received 14 November 2018; revised manuscript received 27 February 2019; published 10 July 2019)

We introduce quantum hypercube states, a class of continuous-variable quantum states that are generated as orthographic projections of hypercubes onto the quadrature phase space of a bosonic mode. In addition to their interesting geometry, hypercube states display phase-space features much smaller than Planck's constant, and a large volume of Wigner negativity. We theoretically show that these features make hypercube states sensitive to displacements at extremely small scales in a way that is surprisingly robust to initial thermal occupation and to small separation of the superposed state components. In a high-temperature proof-of-principle optomechanics experiment we observe, and match to theory, the signature outer-edge vertex structure of hypercube states.

DOI: 10.1103/PhysRevLett.123.020402

Non-Gaussian quantum states are commonly considered as a valuable resource for quantum-information processing [1], tests of fundamental of physics [2,3], and sensing and metrology applications [4,5]. A crucial indicator for how useful a quantum state will be for these applications is how distinguishable it becomes from the initial state after a small displacement. This is closely related to the size of the smallest features in the state's phase space representation [6]. Roughly speaking, two quantum states with smallest features occupying an area on the order of d can become maximally distinguishable for displacements on the order of $\sqrt{d}$. Similarly, the rate of change in distinguishability in response to a displacement—a measure of the state's sensitivity to displacements—is a function of the size of the state's phase-space features. Quantum mechanics generally limits the size of these features to be at least on the order of $\hbar$, which is known as the shot noise or standard quantum limit depending on the area of physics in which it arises.

Yet, quantum theory also provides a way around this limit, and states such as the Schrödinger-cat state [7]—and the more-recently introduced compass state [6,8]—show features at a scale below $\hbar$. States with such *sub-Planck* features have thus attracted significant theoretical attention [8–15] for their potential in sensing applications. However, most of the theory to date has focused on pure states, leaving open the question of how sensitive sub-Planck states will be under realistic conditions.

Here we introduce and study in detail a new class of nonclassical states that we call hypercube states. These states have an intriguing link to geometry in that they are obtained as Petrie-polygon orthographic projections of n cubes [16], see Fig. 1, into phase space, where the polygon vertices correspond to the location of superposed coherent states, and interference fringes in the Wigner function are observed between every pair of vertices, see Fig. 2. This class of states in particular includes the Schrödinger-cat state and the compass state as the lowest-order special cases. All hypercube states exhibit sub-Planck phase-space features that decrease in size with the order of the state, making them an attractive candidate for quantum metrology. We show that hypercube states indeed become distinguishable under progressively smaller displacements with increasing order and, importantly, that this distinguishability is robust to variations in thermal occupation and/or

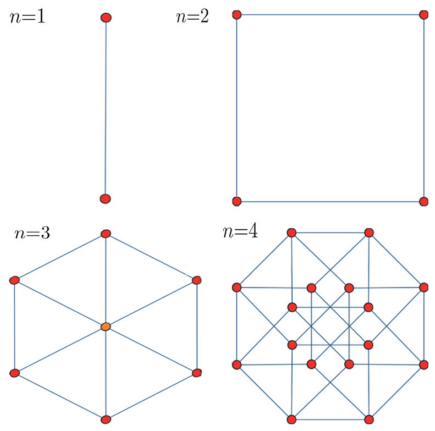

FIG. 1. Petrie polygon orthographic projections of first four n cubes. Red dots represent the projection of a single vertex onto a unique point in phase space, and orange dots the projection of two vertices onto the same point. $n = 1$ is the projection of a line segment; $n = 2$ of a square; $n = 3$ of a cube; and $n = 4$ of a tesseract.

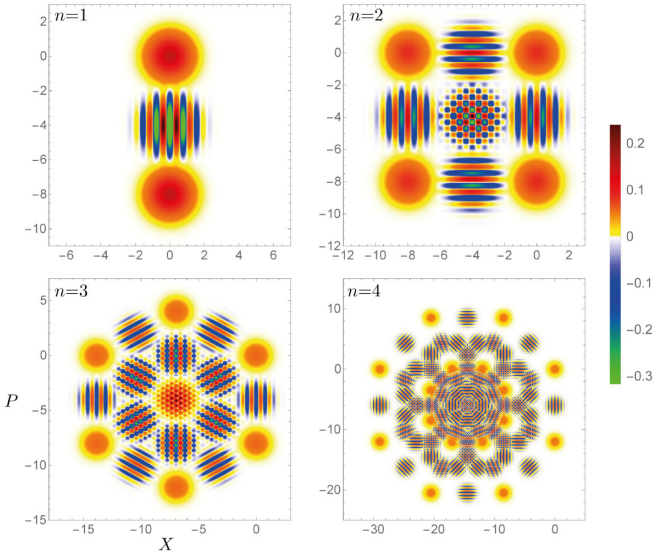

FIG. 2. Density plots of the Wigner functions of the first four hypercube states. All axes are in terms of the ground state width.

the interaction strength of the state for a wide range of realistic experimental parameters. Finally, building on the technique introduced in Ref. [17] we discuss how quantum hypercube states can be prepared in a wide range of state-of-the-art optomechanical experiments. In a proof-of-principle demonstration we experimentally observed the signature of the second-, third-, and fourth-order hypercube states in the high-temperature regime.

Hypercube states.—Mechanical hypercube states are engineered by the sequential application of an instrument or Kraus operator Υ, defined as a superposition of the identity and a displacement, with intermittent phase-space rotations R on the initial mechanical state ρ_{i}. The overall Kraus operator is thus given by

$$\mathcal{Y}_n \propto \prod_n (R(\pi/n)\Upsilon). \tag{1}$$

Here, the rotations are due to the free evolution of the mechanics for durations of $t = T/2n$ that result in phase changes of $\theta = 2\pi t/T = \pi/n$, with T being the period of the mechanical resonator and n being the order of the desired hypercube state. Moreover, $\Upsilon = e^{-|\alpha|^2}\alpha$ $(\mathcal{D}(i\mu/\sqrt{2}) - 1)/\sqrt{2}$, where λ is the wavelength and $\alpha \ll 1$ is the amplitude of the mediating coherent light field, $\mathcal{D}(\beta)$ $(\beta \in \mathbb{C})$ is the mechanical displacement operator, and $\mu = 4\pi x_0/\lambda$ is the interaction strength (equivalent to the optomechanical coupling strength in an optomechanical setting) in which $x_0 = \sqrt{\hbar/m\omega}$ is the mechanical zero-point fluctuation. We note that Υ (and hence $\mathcal{Y}_n$) is obtained by conditioning on the outcome of a photon-counting measurement of the optical field after the radiation pressure interaction, and is thus nonunitary as detailed in the Supplemental Material [18]. The Wigner function phase-space representation [7] of the four lowest order hypercube states when the mechanics starts off from the vacuum are shown in Fig. 2.

ℓ_1-norm sensitivity analysis.—In order to quantify how quickly a displaced quantum state ρ_σ becomes distinguishable from the initial state ρ for small displacements σ, we use the ℓ_1 distance between the corresponding Wigner functions W_ρ and W_{ρ_σ},

$$\ell_1 := \|W_{\rho_\sigma} - W_\rho\|_1 = \int_{-\infty}^{\infty} dx dp |W_{\rho_\sigma}(x,p) - W_\rho(x,p)|,$$

and consider the rate of change $d\ell_1/d\sigma$ of this distance at the point $\sigma = 0$. Importantly, this measure, denoted as ℓ_1 *sensitivity*, can easily be applied in the thermal regime which is a crucial element of this work.

Different regimes of operation can be parametrized by the interaction strength μ and the temperature of the mechanical mode as measured by the average phonon number $\bar{n}$. We are particularly interested in the ℓ_1 sensitivity of hypercube states in three limiting cases: (i) cold, large-coupling: mechanical resonator in the ground state, $\bar{n} = 0$, and $\mu = 6$, 8, and 12, for the second-, third-, and fourth-order hypercube states, respectively; (ii) cold, small-coupling: mechanical resonator in the ground state, $\bar{n} = 0$, and $\mu = 8 \times 10^{-9}$; and lastly (iii) hot, small-coupling: mechanical resonator in a thermal state with $\bar{n} \sim 10^{15}$, and small interaction, $\mu = 8 \times 10^{-9}$, motivated by the proof-of-principle experiment presented at the end of the Letter. The fourth limiting regime of hot-large coupling is less experimentally relevant, because experiments that achieve large coupling between the optical field and resonator can typically cool the resonator very efficiently using laser cooling methods. Nevertheless we do consider how the ℓ_1 sensitivity changes as a strongly coupled resonator warms up, effectively moving from the cold-large towards the hot-large coupled regime, see bottom row of Fig. 3.

Our theoretical analysis of the ℓ_1 sensitivity of a second-order hypercube state transitioning between the above described regimes is summarized in Fig. 3. In the top row of Fig. 3 we show how increasing the interaction strength μ to transition from the small- to the large-coupling regime at low temperature leads to smaller phase-space features and an ℓ_1 sensitivity that increases quadratically with μ for $\mu \lesssim 3$ and linearly for larger μ; see Supplemental Material for details [18]. Note, however, that for any value of μ hypercube states are more sensitive to displacements than a coherent state and maintain significant Wigner negativity (see Fig. S4 [18]). Interestingly, for very small interaction strengths the symmetry around the position axis breaks, meaning that at some values the state is more sensitive to displacements in momentum than in position, or vice versa; see Supplemental Material for details [18].

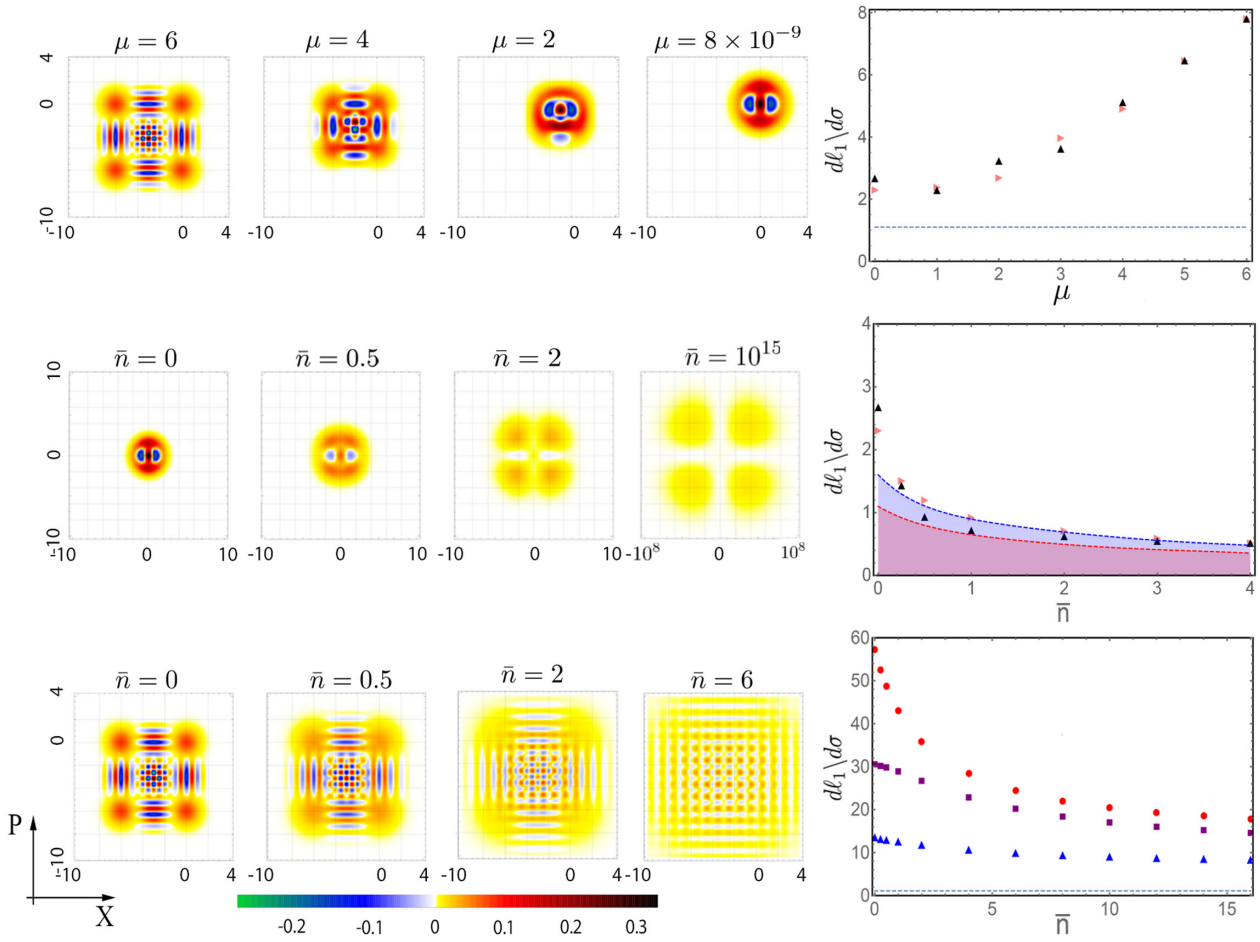

FIG. 3. $n = 2$ hypercube state for a mechanical resonator as produced by our scheme. Left-hand side: Theoretical density plots of the Wigner function in position-momentum ($X - P$) phase space. The color bar on the bottom shows the value of the Wigner function where blue and green indicate areas of negative quasiprobability. All axes are in terms of the ground state width. Right-hand side: Corresponding ℓ_1 sensitivity, $d\ell_1/d\sigma$, vs position or momentum displacement plots (position, pink horizontal triangles) or (momentum, black vertical triangles). The blue dotted line indicates ℓ_1 sensitivity of a coherent state at zero temperature. Top row: Cold temperature: small $\rightarrow$ large coupling ($\bar{n} = 0$; $\mu = 6 \rightarrow \mu = 8 \times 10^{-9}$). Middle row: small coupling: cold $\rightarrow$ hot temperature ($\mu = 8 \times 10^{-9}$; $\bar{n} = 0 \rightarrow \bar{n} = 10^{15}$; the colors in the last panel are scaled by 10^8 in accordance with the axis scaling). The ℓ_1 sensitivity plot shows that even hypercube states with vanishing separation of coherent states are more sensitive than thermal states (red-shaded region) and at least as sensitive as squeezed (3 dB) thermal states (blue shaded region) with the same mean phonon number and more sensitive than a ground state coherent state for $\bar{n} \lesssim 0.5$. Bottom row: Large coupling: cold $\rightarrow$ warm temperature ($\mu = 6$; $\bar{n} = 0 \rightarrow \bar{n} = 6$). $n = 2$ hypercube states are shown by blue triangles; for comparison, $n = 3$ and $n = 4$ hypercube states are shown, respectively, by purple squares and red circles. Note that in the right plot $\mu = 12$ was used to ensure clear separation of coherent states across all the orders of the hypercube state.

The middle row of Fig. 3 shows the transition between the small-coupling regimes and that as the temperature increases Wigner negativity and smaller scale features disappear and the outer-edge vertex structure becomes the dominant feature. As a result, the ℓ_1 sensitivity of the states decreases exponentially with temperature, see Supplemental Material for details [18]. Interestingly, however, hypercube states show an ℓ_1 sensitivity at least as high as 3 dB-squeezed coherent states of the same average phonon number even in the regime where $\mu \ll 1$. For low temperatures of $\bar{n} \lesssim 0.25$, hypercube states are more sensitive than the corresponding squeezed states.

In the bottom row of Fig. 3 we increase temperature in the cold large-coupling regime. Here we see that periodic and symmetric sub-Planck features are visible for $0 < \bar{n} \leq 6$. In fact, they exist even at much higher temperatures. The ℓ_1-sensitivity plot on the right side of the row highlights both that, in this regime, the ℓ_1 sensitivity is robust to temperature increases, and that it increases substantially with the order of the hypercube. These results apply equally to displacements along the position or momentum axis.

Experimental method and results.—Our experimental method utilizes a series of n interactions between an optical field and mechanical resonator [17], followed by single

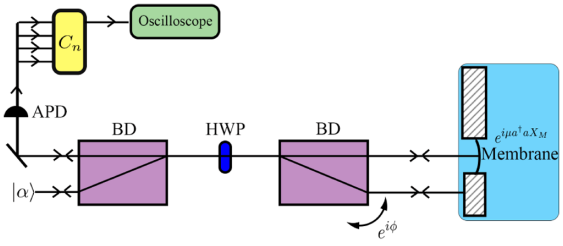

FIG. 4. A weak coherent state $|\alpha\rangle$ is inserted and split using a half wave plate (HWP) and a beam displacer (BD) into two arms of a folded interferometric setup. The optical field in the top arm interacts with a membrane mechanical resonator via radiation pressure, described by $e^{i\mu a_1^\dagger a_1 X_M}$. Here a and $a^\dagger$ are the annihilation and creation operators, μ is the optomechanical coupling strength, and X_M is the mechanical position operator. The bottom arm interacts with the static frame of the membrane, obtaining a controllable phase shift $e^{i\phi}$, which we set to $\phi = \pi$. Post these interactions, the optical fields in both arms are interfered, split into the polarization components, and detected in an avalanche photon detector (APD). The detector signal is then split into two, three, or four paths depending on whether detection of a second-, third-, or fourth-order hypercube is being made; with each path past the first adding a time delay of $T/2n$. Coincidence counting between the paths is made at C_n, and upon detection of a coincidence event an oscilloscope is triggered to record a trace of the membrane's position from the back (not shown).

photon detection to create an nth order hypercube state within the mechanical resonator. Prior to the interaction, each single photon is in a quantum superposition of being incident, and not incident, on a mechanical resonator. Interaction of the mechanical resonator and a photon thereby puts the mechanical resonator in a quantum superposition of receiving, and not receiving, a momentum kick due to the radiation pressure applied by the photon incident on the resonator. This interaction effectively applies Υ and hence a series of photons prepared this way, with time $t = T/2n$ between successive photons acts to apply Eq. (1) to the state of mechanical resonator. A schematic of the setup, with further details in the caption is shown in Fig. 4.

We now introduce the experimental results from implementing our method in the hot small-coupling regime with a 100 ng ($\simeq 10^{16}$ atoms) mechanical resonator. To ensure a large physical displacement that can be easily measured, the resonator is driven with a piezo (in order to create a Gaussian state in phase space the piezo drive voltage is Chi-distributed due to the drive voltage coupling to $\sqrt{X^2 + P^2}$). This gives the resonator an effective thermal occupation of $\bar{n} = 10^{15}$. The mechanical resonator was coupled to 795 nm light, with the application of the measurement operator $\mathcal{Y}_n$ heralded by n sequential single-photon detections. Detection of photons separated by $T/2n$ was accomplished by splitting the electronic signal from the photon detector into multiple paths of varying lengths and then looking for coincidences between the paths, see Supplemental Material for details [18].

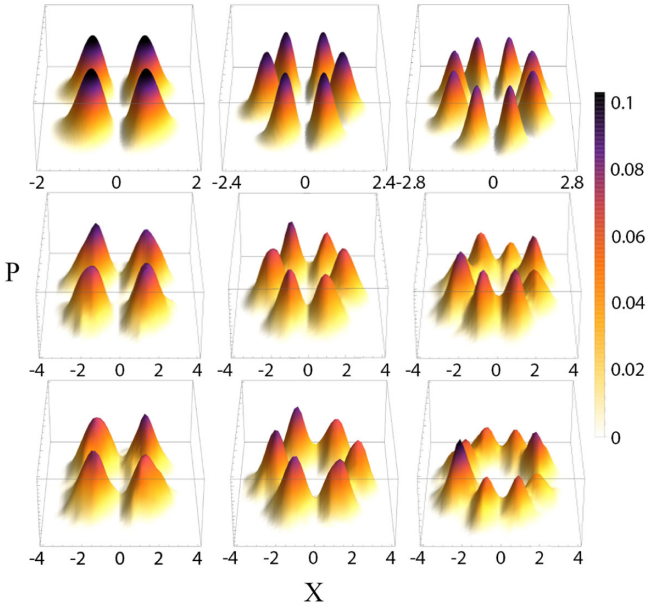

FIG. 5. Normalized probability densities of hypercube states; left to right columns correspond to second-, third- and fourth-order hypercube states. Top row: Ideal densities, from Eq. (1): Populations match the outer ring of vertices of the Petrie projections in Fig. 1; quantum features such as sub-Planck structure are absent due to high temperature. Middle row: Densities predicted from a model that accounts for experimental drift, timing uncertainties, and counting statistics; see Supplemental Material [18]. Note the predicted variations in peak height, width, and shape. Bottom row: Measured probability densities, the Bhattacharyya coefficient (a classical analogue of the fidelity) between the middle row of density plots and the experimentally measured density plots are 0.95 ± 0.02, 0.90 ± 0.02, and 0.82 ± 0.02 for the second-, third-, and fourth-order hypercube states, respectively. The uncertainties represent 1 standard deviation obtained from the statistical uncertainties in determining the values of X and P. The signature of hypercube states in the thermal regime—the ring of outer-edge-vertices—is clearly visible in all plots. All axes are in units of $\lambda_R/4 = 158.2$ nm, where λ_R is the readout wavelength used to measure the mechanical resonators' phase-space position.

Figure 5 displays, and compares to theory, our experimental measurements of hypercube states of orders $n = 2$, $n = 3$, and $n = 4$ in the hot small-coupling regime. The top row of Fig. 5 shows the theoretical expectation in the ideal case of no experimental limitations: probability densities that reproduce the outer-ring of vertices of the Petrie projections in Fig. 1, and that do not contain quantum features, or sub-Planck structure—as expected due to the high temperature. These plots are generated by applying $\mathcal{Y}_n$ of Eq. (1). The middle row of Fig. 5 adds modeling of the major experimental limitations present; namely, drift in the interferometer setting ϕ, experimental timing uncertainties when applying $R(\pi/2n)$, and variations from the mean due to counting statistics and displays notable variations in the height, width, and shape of the peaks in the probability

densities; see the Supplemental Material for details [18]. The bottom row shows our measured results which show the same features—there is excellent agreement between the model predictions and our experiments (see the caption of Fig. 5 quantification of agreement).

Hypercube states establish a strong connection to geometry for continuous-variable quantum states, as well as providing an avenue for sub-Planck sensing over a surprisingly large range of experimental parameters. Given their potential, and the pivotal role geometry has played in the field of discrete-variable quantum information processing for problems such as measurement-based quantum computing and quantum error correction; we expect hypercube states will inspire diverse applications in fields such as quantum sensing, quantum information theory and quantum foundations [3,22,23]. To achieve these applications will require an amalgamation of current technologies for precision quadrature measurements at the sub-Planck scale [24–26], and cooling a mechanical resonator to close to the ground state [27].

We acknowledge support from the Australian Research Council (ARC) via the Centre of Excellence for Engineered Quantum Systems (EQUS, CE170100009), a Discovery Project for M. R. V. (DP140101638) and a Discovery Early Career Researcher Award for J. C. (DE160100356); the Engineering and Physical Sciences Research Council (EP/N014995/1); and the University of Queensland by a Vice-Chancellor's Senior Research and Teaching Fellowship for A. G. W. This project has received funding from the European Union's Horizon 2020 research and innovation programme under the Marie Skłodowska Curie Grant Agreement No. 801110 and the Austrian Federal Ministry of Education, Science and Research (BMBWF). F. S. acknowledges support and resources provided by the Sêr SAM Project at Swansea University, an initiative funded through the Welsh Government's Sêr Cymru II Program (European Regional Development Fund).

[1] M. Mirrahimi, Z. Leghtas, V. V. Albert, S. L. Touzard, R. J. Schoelkopf, L. Jiang, and M. H. Devoret, New J. Phys. **16**, 045014 (2014).
[2] S. Bose, K. Jacobs, and P. L. Knight, Phys. Rev. A **59**, 3204 (1999).
[3] W. Marshall, C. Simon, R. Penrose, and D. Bouwmeester, Phys. Rev. Lett. **91**, 130401 (2003).
[4] P. Walther, J.-W. Pan, M. Aspelmeyer, R. Ursin, S. Gasparoni, and A. Zeilinger, Nature (London) **429**, 158 (2004).
[5] M. W. Mitchell, J. S. Lundeen, and A. M. Steinberg, Nature (London) **429**, 161 (2004).
[6] W. H. Zurek, Nature (London) **412**, 712 (2001).
[7] U. Leonhardt, in *Measuring the Quantum State of Light*, Cambridge Studies in Modern Optics (Cambridge University Press, New York, 1997).
[8] F. Toscano, D. A. R. Dalvit, L. Davidovich, and W. H. Zurek, Phys. Rev. A **73**, 023803 (2006).
[9] G. S. Agarwal and P. K. Pathak, Phys. Rev. A **70**, 053813 (2004).
[10] D. A. R. Dalvit, R. L. de Matos Filho, and F. Toscano, New J. Phys. **8**, 276 (2006).
[11] S. Ghosh, A. Chiruvelli, J. Banerji, and P. K. Panigrahi, Phys. Rev. A **73**, 013411 (2006).
[12] U. Roy, S. Ghosh, P. K. Panigrahi, and D. Vitali, Phys. Rev. A **80**, 052115 (2009).
[13] S. Choudhury and P. K. Panigrahi, AIP Conf. Proc. **1384**, 91 (2011).
[14] L. Praxmeyer, C.-C. Chen, P. Yang, S.-D. Yang, and R.-K. Lee, Phys. Rev. A **93**, 053835 (2016).
[15] K. Jacobs, R. Balu, and J. D. Teufel, Phys. Rev. A **96**, 023858 (2017).
[16] M. W. Davis, *The Geometry and Topology of Coxeter Groups (LMS-32)* (Princeton University Press, Princeton, 2008).
[17] M. Ringbauer, T. J. Weinhold, L. A. Howard, A. G. White, and M. R. Vanner, New J. Phys. **20**, 053042 (2018).
[18] See Supplemental Material at http://link.aps.org/supplemental/10.1103/PhysRevLett.123.020402 for additional experimental and theory details, which includes Refs. [19–21].
[19] F. Shahandeh and M. R. Bazrafkan, J. Phys. A **45**, 155204 (2012).
[20] A. Kenfack and K. Życzkowski, J. Opt. B **6**, 396 (2004).
[21] V. Veitch, N. Wiebe, C. Ferrie, and J. Emerson, New J. Phys. **15**, 013037 (2013).
[22] C. Anastopoulos and B. L. Hu, Classical Quantum Gravity **32**, 165022 (2015).
[23] A. Bassi, K. Lochan, S. Satin, T. P. Singh, and H. Ulbricht, Rev. Mod. Phys. **85**, 471 (2013).
[24] M. R. Vanner, I. Pikovski, and M. S. Kim, Ann. Phys. (Berlin) **527**, 15 (2015).
[25] M. R. Vanner *et al.*, Proc. Natl. Acad. Sci. U.S.A. **108**, 16182 (2011).
[26] F. Shahandeh and M. Ringbauer, Quantum **3**, 125 (2019).
[27] M. Rossi, D. Mason, J. Chen, Y. Tsaturyan, and A. Schliesser, Nature (London) **563**, 53 (2018).